Navigation Systems Based On Single Pseudo-Range Measurements: Design and Experimental Evaluation

João Manuel Franco
jmlacfranco@gmail.com

Instituto Superior Técnico, Universidade de Lisboa, Portugal

January 2021

Abstract

This thesis refers to acoustic navigation systems based on single range measurements. The difficulty of accurately determining the speed of sound on the propagation medium, a matter of special relevance in sub aquatic and aeronautic applications, is addressed by considering that the range measurements acquired by the system are affected by an unknown multiplicative coefficient. The inherent nonlinear nature of the navigation problem is tackled by performing state augmentation. The discrete-time linear system obtained with this approach is shown to be observable and a Kalman filter is employed in order to obtain state estimates with globally exponentially stable error dynamics. Simulations, assuming noisy environments, are conducted to compare this solution with common nonlinear estimation techniques, namely the extended Kalman filter and the unscented Kalman filter. The latter are shown to obtain comparable results, but fail to provide global convergence guarantees. Monte Carlo simulations supply further insights on filtering performances. Finally, experiments in a controlled environment are carried out, attesting the applicability of the proposed solution.
Keywords: single ranges, navigation, speed of sound, Kalman filter, Bayesian Cramér-Rao bound, Monte Carlo simulations

1. Introduction

The need for underwater vehicle (UV) positioning has increased in the recent years. Breakthroughs in the field of artificial intelligence have lead to a significant burst of autonomous UV applications. Other engineering quests, such as offshore energy production and seafloor mapping, often require the operation of UVs to achieve prosperous results.

Nowadays, acoustic systems are the standard for accurate underwater navigation. Three major classes of systems are available for position determination. These are the long baseline (LBL) systems, the short baseline (SBL) systems, and the ultra short baseline (USBL) systems. Each of these solutions comprises its own specific implementation and expected performance, but they all have in common the fact that, like in the global positioning system (GPS), multiple waves, from multiple transponders, are propagated between the navigation system and the user. From these multiple range measurement systems a series of problems arise. One of them, and, probably, the most important one is the fact that multiple range measurements, by requiring multiple transponders, amount to increasing system complexity and deployment costs. Another problem is the fact that a fail in one or more transponders might lead to the system being rendered useless, since common multilateration techniques might become compromised. A way to solve these two issues is to use just one transponder capable of performing the same task as all the systems mentioned before. Having this in mind, acoustic navigation based in single range measurements has attracted the interest of the scientific community in the recent years.

One of the first works addressing the concept of underwater navigation based on single range measurements to a stationary beacon dates back to the beginning of the century [1]. The author proposes a solution to overcome the known limitations of dead-reckoning navigation by combining a high performance dead-reckoning system with an innovative synthetic long baseline. The latter consisting on a set of consecutive discrete-time range measurements from the moving vehicle to a stationary beacon. Kalman filtering was applied to a linearized version of the system dynamics. In [2], the navigation problem is addressed with special concerns for known current velocities. System linearization is performed and an extended Kalman filter is used to produce state estimates, but no guarantees of global asymptotically stable error dynamics are pro-

vided. The same strategy was then employed in [3] and [4], where unknown currents are considered. In [5], algebraic methods are used to study system observability and to perform state estimation. A state augmentation approach, which yields state estimates with globally exponentially stable (GES) error dynamics, is brought forward in [6]. Also motivated by state augmentation processes, the authors in [7] propose a novel estimator based on the least entropy-like estimator [8] capable of dealing with unavoidable measurement outliers.

A very important factor when considering acoustic range measurements for navigation purposes is that the speed of sound needed to obtain those measurements tends to vary according to specific environment conditions. Studies combining the concept of single range measurement navigation and the difficulties of proper speed of sound determination have recently emerged. In [9] speed of sound is explicitly estimated in a single pseudo-range measurement navigation/source localization problem, where state augmentation is the preferred route. The new system obtained with this technique is inspected for observability purposes and a Kalman filter provides state estimates with GES error dynamics. The work [10] proposes a solution to overcome the errors associated with a misidentified effective sound velocity (ESV) in navigation models. The researchers treat ESV as a model parameter and use the expectation maximization method to obtain estimates of this unknown parameter. The overall single-transponder navigation method also incorporates a Kalman filter. To tackle noise sensitivity and initial vehicle position errors, which might lead to fails in the two previous solutions, [11] treats the ESV as a random variable with unknown properties. Both the ESV and its statistical properties are then estimated resorting to a variational Bayesian approximation method.

In this thesis the most simple form of underwater navigation in terms of setup and deployment, i.e., navigation with a single fixed transponder, is studied. The notion of an unknown speed of sound in the medium is also a subject of this work. Along these lines, range measurements acquired from a transponder system are considered to be affected by an unknown multiplicative factor. Taking this into consideration, a nonlinear discrete-time system representative of the navigation problem is derived, and estimates of the position of the vehicle as well as the speed of sound unknown multiplicative coefficient are obtained with the solution proposed in [9]. In order to compare the novel solution with common nonlinear estimation techniques, an extended Kalman filter (EKF) and an unscented Kalman filter (UKF) are also employed to provide vehicle and speed of sound estimates. Filtering parameters are subject to an optimization process called Bayesian optimization (BO) . Extensive Monte Carlo simulations provide further comprehension of the performance of each filtering solution by allowing the determination of bias in the estimation process as well as estimation error covariance. Finally, experiments in a controlled environment are performed, attesting the applicability of the new solution.

1.1. Notation

Vectors are represented in bold with each component appearing as an upper index. For example, $\mathbf{p}^x$, $\mathbf{p}^y$, and $\mathbf{p}^z$ represent the first, second, and third components of a vector $\mathbf{p} \in \mathbb{R}^3$. The bold upper case is reserved for matrices such as a $n \times n$ identity matrix, $\mathbf{I}_n$, or the zeros matrix, $\mathbf{0}_n$. A block diagonal matrix is represented by $diag(\mathbf{A}_1, ...\mathbf{A}_n)$. The inner product of $\mathbf{p} \in \mathbb{R}^3$ and $\mathbf{q} \in \mathbb{R}^3$ is $\mathbf{p} \cdot \mathbf{q}$. Finally, the special orthogonal group of dimension n is represented as $SO(n)$.

2. Problem statement

The navigation systems proposed in this thesis foresee the use of a single fixed acoustic transponder to acquire discrete-time range measurements to an operating vehicle. The aforementioned systems rely on a basic principle of wave propagation which states that, in the absence of a variable speed of sound, the distance traveled by the acoustic wave is equal to its speed of propagation in the medium multiplied by the time it took for the wave to travel said distance. The problem regarding this simple formulation is that the speed of sound considered to compute distances might not correspond to the true value, be it from inaccurate determination or complete lack of information. Having this in mind, one can assume that the range measurements provided by the system are affected by an unknown multiplicative factor. It is also assumed that these systems comprise the use of other navigation equipment such as a Doppler velocity log (DVL) and an attitude and heading reference system (AHRS) to determine the inertial speed of the vehicle and its orientation relative to a reference frame, respectively.

2.1. System dynamics

As usual in navigation systems, consider the existence of $\{I\}$, a local coordinate inertial reference frame, and $\{B\}$, a coordinate frame that moves with the vehicle along its motion through the medium, the so-called body-fixed frame.

The variation of the inertial position of the vehicle, $\dot{\mathbf{p}}(\mathbf{t}) \in \mathbb{R}^3$, can be written as

$$\dot{\mathbf{p}}(t) = \mathbf{R}(t)\mathbf{v}(t), \tag{1}$$

where $\mathbf{R}(t) \in SO^3$ is the rotation matrix from $\{B\}$ to $\{I\}$ and $\mathbf{v}(t)$ is the velocity of the vehicle rela-

tive to $\{I\}$, expressed in body-coordinates. In this thesis, it is assumed that the vehicle is capable of acquiring both the rotation matrix $\mathbf{R}(t)$ and the velocity $\mathbf{v}(t)$. In practice, the first is usually obtained through the aforementioned AHRS and the second through the DVL if the later has established bottom-lock.

Discrete-time range measurements to a stationary beacon, $r(k)$, can be obtained through

$$r(k) = v_s(t_k) \parallel \mathbf{s} - \mathbf{p}(t_k) \parallel \tag{2}$$

where $\mathbf{s} \in \mathbb{R}^3$ is the inertial position of the beacon, t_k is the sampling instant, defined with respect to the sampling period $T > 0$ and the initial time t_0, as $t_k := t_0 + kT$, $k \in \mathbb{N}$. Finally, $v_s(t_k) > 0$ denotes the strictly positive scaling factor that accounts for the uncertainties in the speed of propagation of the acoustic waves.

Considering, for the sake of simplicity, that the velocity of propagation in the medium does not change over time, the previous equations can be condensed to represent the system dynamics as

$$\begin{cases} \dot{\mathbf{p}}(t) = \mathbf{R}(t)\mathbf{v}(t) \\ \dot{v_s}(t) = 0 \\ r(k) = v_s(t_k) \parallel \mathbf{s} - \mathbf{p}(t_k) \parallel . \end{cases} \tag{3}$$

The above equations depict a continuous nonlinear system that can be discretized as

$$\begin{cases} \mathbf{p}(t_{k+1}) = \mathbf{p}(t_k) + \mathbf{u}(t_k) \\ v_s(t_{k+1}) = v_s(t_k) \\ r(k) = v_s(t_k) \parallel \mathbf{s} - \mathbf{p}(t_k) \parallel, \end{cases} \tag{4}$$

where the system input, $\mathbf{u}(t_k)$, accounts for the traveled distance, in inertial coordinates, between consecutive pseudo-range measurements. It can be computed through the integral

$$\mathbf{u}(t_k) = \int_{t_k}^{t_{k+1}} \mathbf{R}(\tau)\mathbf{v}(\tau)d\tau. \tag{5}$$

The problem addressed in this thesis is that of estimating $\mathbf{p}(t_k)$ and $v_s(t_k)$ assuming that both the pseudo-range measurements $r(k)$ and the system input $\mathbf{u}(t_k)$ are available at each time step k.

3. Linear Kalman filter

To perform state estimation on the system under study, a novel solution proposed in [9] was implemented. This consists primarily in performing state augmentation, thus obtaining a new augmented system. State estimates are then obtained using a simple linear Kalman filter (LKF).

3.1. Theoretical foundation

Consider a generic system of the form

$$\begin{cases} \mathbf{x}_1(k+1) = \mathbf{x}_1(k) + \mathbf{u}(k) \\ x_2(k+1) = x_2(k) \\ r(k+1) = x_2(k+1) \parallel \mathbf{x}_1(k+1) \parallel . \end{cases} \tag{6}$$

This formulation is equivalent to (4) if $\mathbf{x}_1(k)$ and $x_2(k)$ are defined as

$$\begin{cases} \mathbf{x}_1(k) := \mathbf{p}(k) - \mathbf{s} \\ x_2(k) := v_s(k). \end{cases} \tag{7}$$

Assumption 1: All pseudo-ranges, $r(k)$, are greater than zero, i.e., $r(k) > 0$ for all k.

By applying the following state augmentation process, new system states are defined as

$$\begin{cases} \mathbf{z}_1(k) := x_2^2(k)\mathbf{x}_1(k) \\ z_2(k) := x_2^2(k) \\ z_3(k) := r(k). \end{cases} \tag{8}$$

Regarding $\mathbf{z}_1(k)$ and $z_2(k)$, these have a very easy-to-infer evolution which, when taking into account (6) and (8), can be stated as

$$\begin{cases} \mathbf{z}_1(k+1) := \mathbf{z}_1(k) + z_2(k)\mathbf{u}(k) \\ z_2(k+1) := z_2(k). \end{cases} \tag{9}$$

The evolution of the third state is, after some considerations and substitutions (here omitted due to space limitations), given by

$$\begin{aligned} z_3(k+1) =& 2\frac{\mathbf{u}(k)}{r(k+1)} \cdot \mathbf{z}_1(k) + \frac{\parallel \mathbf{u}(k) \parallel^2}{r(k+1)} z_2(k) \\ &+ \frac{r(k)}{r(k+1)} z_3(k). \end{aligned} \tag{10}$$

Now, notice that (9) and (10) linearly describe time-step transitions of $\mathbf{z}_1(k)$, $z_2(k)$, and $z_3(k)$ since both $\mathbf{u}(k)$ and $r(k)$ can be viewed as system inputs, which are available over time. Also, notice that $z_3(k) := r(k)$ can be viewed as a system measurement. Having this in mind and defining the state vector

$$\mathbf{z}(k) := \begin{bmatrix} \mathbf{z}_1(k) & z_2(k) & z_3(k) \end{bmatrix}^T, \tag{11}$$

the system dynamics can be written in the form

$$\begin{cases} \mathbf{z}(k+1) = \mathbf{A}(k)\mathbf{z}(k) \\ y(k+1) = \mathbf{C}\mathbf{z}(k), \end{cases} \tag{12}$$

with

$$\mathbf{A}(k) = \begin{bmatrix} \mathbf{I}_3 & \mathbf{u}(k) & \mathbf{0}_{3\times 1} \\ \mathbf{0}_{1\times 3} & 1 & 0 \\ 2\frac{\mathbf{u}^T(k)}{r(k+1)} & \frac{\|\mathbf{u}(k)\|^2}{r(k+1)} & \frac{r(k)}{r(k+1)} \end{bmatrix} \in \mathbb{R}^{5\times 5}$$

and

$$\mathbf{C} = \begin{bmatrix} \mathbf{0}_{1\times 3} & 0 & 1 \end{bmatrix} \in \mathbb{R}^{1\times 5}.$$

3.2. Observability analysis

The two measurements needed to determine the dynamics matrix $\mathbf{A}(k)$ can be viewed as discrete functions of time, since they are assumed to be available at every time instant k. For this reason, the system (12) can be seen as a discrete-time linear time-varying system from an observability perspective [12]. Theorem 1 refers to the observability of the system (12).

Theorem 1[9]: Assuming that the matrix $\mathbf{L}(k_a)$, defined for time instant $k_a \geq 0$ as

$$\mathbf{L}(k_a) := \begin{bmatrix} \mathbf{L}_0(k_a) \\ \vdots \\ \mathbf{L}_3(k_a) \end{bmatrix} \in \mathbb{R}^{4\times 4},$$

where

$$\mathbf{L}_i(k_a) := \begin{bmatrix} 2\sum_{j=0}^{i} \mathbf{u}(k_a+j) \\ \| \sum_{j=0}^{i} \mathbf{u}(k_a+j) \|^2 \end{bmatrix}^T \in \mathbb{R}^{1\times 4},$$

is a full rank one, i.e.,

$$rank(\mathbf{L}(k_a)) = 4, \tag{13}$$

then the initial state $\mathbf{z}(k_a)$ is uniquely determined by the input $\{ \mathbf{u}(k) : k = k_a, ..., k_a + 4\}$ and the output $\{ \mathbf{y}(k) : k = k_a, ..., k_a + 4\}$. This means that system (12) is observable in the time interval $[k_a, k_a + 5]$.

Nevertheless, showing that system (12) is observable is not enough to prove that state estimates of this relate to estimates of the original nonlinear system (6), since the state augmentation process required the output $r(k) = x_2(k)||x_1(k)||$ to be discarded and new artificial states to be created. The following theorem proves this relation.

Theorem 2[9]: If (13) holds, then :

1. The initial state of the original nonlinear system (6), $(\mathbf{x}_1(k_a), x_2(k_a))$, is uniquely determined by the input $\{ \mathbf{u}(k) : k = k_a, ..., k_a + 4\}$ and the output $\{ r(k) : k = k_a, ..., k_a+4\}$. This is the same as saying that the nonlinear system (6) is observable in the time interval $[k_a, k_a+5]$.

2. There is a match between the initial conditions of both the augmented (12) and the original (6) systems, i.e.,

$$\begin{cases} \mathbf{z}_1(k_a) = x_2^2(k_a)\mathbf{x}_1(k_a) \\ z_2(k_a) = x_2^2(k_a) \\ z_3(k_a) = x_2(k_a)||\mathbf{x}_1(k_a)|| \end{cases} \tag{14}$$

The proof of both Theorems 1 and 2 is given in [9].

3.3. Linear Kalman filter

Under the conclusions obtained in the previous sections, a Kalman filter was employed to perform state estimation on system (12). The estimates obtained with this solution will show globally exponentially stable (GES) error dynamics if the system (12) is shown to be uniformly completely observable [13]. In the previous subsection it was only shown that the system is observable, but an identical, yet more space consuming, process could be employed to prove uniform complete observability.

Recall the augmented system (12) for which the LKF provides state estimates. The estimated state $\mathbf{z}(k)$ does not correspond directly to the pursued estimates of the vehicle position, $\mathbf{p}(k)$, and the speed of sound multiplicative coefficient, $v_s(k)$. To obtain those, the following assumptions are needed.

Assumption 2: The speed of sound multiplicative factor, $v_s(k) = x_2(k)$, is comprehended between a maximum and a minimum value, $V_M > 0$ and $V_m > 0$, respectively, as given by

$$V_m \leq x_2(k) \leq V_M. \tag{15}$$

Assumption 3: The state tied to vehicle position, $\mathbf{x}_1(k)$, is norm-bounded.

Possessing estimates of $\mathbf{z}(k)$, the speed of sound multiplicative coefficient estimates, $\hat{v}_s(k)$, can be determined by

$$\hat{v}_s(k) = \hat{x}_2(k) = \begin{cases} V_m, & \hat{z}_2(k) < V_m^2 \\ \sqrt{\hat{z}_2(k)}, & V_m^2 \leq \hat{z}_2(k) \leq V_M^2 \\ V_M, & \hat{z}_2(k) > V_M^2, \end{cases} \tag{16}$$

and the vehicle position estimates, $\hat{\mathbf{p}}(k)$, by

$$\hat{\mathbf{p}}(k) = \hat{\mathbf{x}}_1(k) + \mathbf{s} = \frac{\hat{\mathbf{z}}_1(k)}{\hat{x}_2(k)} + \mathbf{s}. \tag{17}$$

Furthermore, it can be shown that, as estimates of $\mathbf{z}(k)$ have GES error dynamics, then estimates of speed of sound multiplicative coefficient and position also have GES error dynamics. The proof of this statement is shown in [12, Proposition 1].

4. Simulations

To assess the performance of the novel solution, simulations were carried out in the Matlab™ environment. The results are compared to those obtained when using an extended Kalman filter and an unscented Kalman filter. To better determine the performance of the filtering solutions, Monte Carlo simulations were conducted. This method is useful to detect possible filter bias. Also, Monte Carlo simulations allow for the determination of error standard deviations which, when compared to the lower bound provided by the Bayesian Cramér-Rao Bound (BCRB) [6, Section V], grant further insights of filtering performance.

The trajectory described by the vehicle was created by determining a set of waypoints in the three-dimensional space. The aforementioned set was obtained by consecutively adding inertial position variations to the trajectory already described. In order to avoid valueless results of the filtering solutions, a rich trajectory, i.e., one without straight lines and lack of changes in direction, was preferred. The variation of each position component $(\Delta\mathbf{p}^x, \Delta\mathbf{p}^y, \Delta\mathbf{p}^z)$, in meters, was modeled as

$$\begin{cases} \Delta\mathbf{p}^x(k) = cos\left(\frac{2\pi}{30}kT\right) \\ \Delta\mathbf{p}^y(k) = cos\left(\frac{\pi}{10}kT + \frac{\pi}{6}\right) \\ \Delta\mathbf{p}^z(k) = cos\left(\frac{2\pi}{45}kT + \frac{\pi}{9}\right), \end{cases} \tag{18}$$

where $k \in \mathbb{N}$ represents the time step and T the update rate used to compute the position variations. Assuming new positions are determined at a frequency of 1 Hz, it follows that $T = 1$s. Each trajectory was limited to 4000 seconds (approximately one hour). The initial inertial position of the vehicle was set to the origin of the inertial reference frame, i.e., $\bar{\mathbf{p}}_0 = \begin{bmatrix} 0 & 0 & 0 \end{bmatrix}^T$. A tree-dimensional view of the trajectory is presented in Fig. 1.

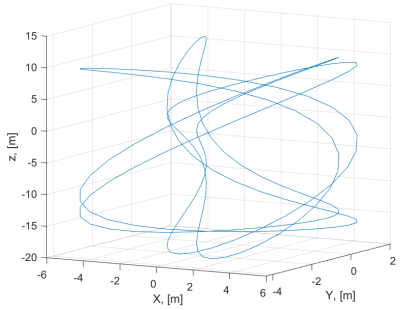

Figure 1: Vehicle trajectory

The pseudo-ranges, $r(k)$, were obtained by computing the euclidean distance between the true vehicle position, $\bar{\mathbf{p}}(t_k)$, and the position of the fixed beacon, $\mathbf{s}$, and then multiplying it by the coefficient $v_s(t_k)$. The latter was initialized with a value of 1.1, and, although it is not expressed in (4), its evolution was assumed to be corrupted by additive zero-mean white Gaussian noise with a standard deviation of 0.01 for BCRB determination purposes. This difference concerns the fact that (4) is a deterministic model, whereas in practice one aims to be able to estimate slowly time-varying parameters. Pseudo-ranges are assumed to be available at a frequency of 1 Hz, the same frequency used to create the trajectory waypoints. The position variation integral, $\mathbf{u}(k)$, was assumed as equal to the position variations used to determine the trajectory of the vehicle, $\Delta_{\mathbf{p}}(k)$. This implies that, with the exception of measurement noise, the integral would be perfectly determined by the sensors on board the vehicle.

Both measurements were assumed to be corrupted with additive zero-mean white Gaussian noise with the standard deviations present in Table 1.

Measure	Standard deviation [m]
$r(k)$	10^{-2}
$\mathbf{u}(k)$	5×10^{-2}

Table 1: Standard deviation of the noise

4.1. Linear Kalman filter

Concerning the LKF, the initial estimation parameters $\hat{\mathbf{x}}_0$ and $\mathbf{P}_0$ were arbitrarily chosen to exemplify the goodness of the solution. Furthermore, process and measurement noise covariance matrices, $\mathbf{Q}_k$ and $\mathbf{R}_k$ respectively, were obtained via the Bayesian optimization algorithm [14]. All the parameters, except for the initial state estimate, are portrayed in Table 2.

Parameter	Value
$\mathbf{P}_0$	I_5
$\mathbf{Q}_k$	$diag(0.207\mathbf{I}_3, 6.466 \times 10^{-5}, 0.876)$
$\mathbf{R}_k$	0.533

Table 2: LKF parameters

The initial state estimate vector $\hat{\mathbf{x}}_0 = \begin{bmatrix} 100 & 141.42 & 141.42 & 1.0 & 100 \end{bmatrix}^T$ was used to feed the filter. This corresponds to an initial estimate where the norm of the position of the vehicle is incorrect by approximately 200 meters, the sound speed multiplicative factor by 0.1, and the range by 100 meters. The convergence of the position and speed of sound coefficient errors are shown in Figures 2 and 3. The novel solution is able to lead the estimation errors to zero quite rapidly, while showing a good steady-state performance, with the norm of position error being consistently below 0.5 meters. Due to space limitations, no more results regarding even higher initial condition errors are shown. Nevertheless, it was observed that, for the noise properties assumed and within the considered simulation length, error convergence was guaranteed up to initial absolute position errors of more than 1000Km.

4.2. Extended Kalman filter

Two initial conditions were used to feed the extended Kalman filter. The tuning of the parameters was also performed resorting to the BO algorithm, being the results of this process shown in Table 3, along with the initial error covariance matrix.

Figures 4 and 5 show the evolution of the position estimation error, as well as that of the speed

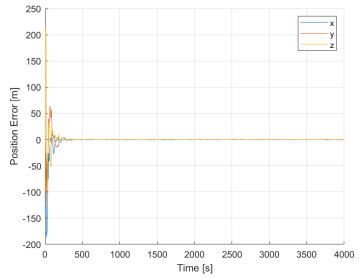

Figure 2: LKF position estimation error

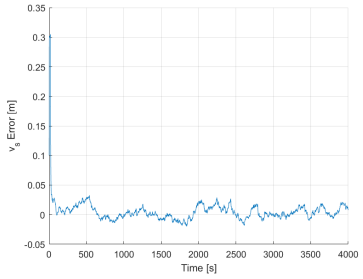

Figure 3: LKF speed of sound coefficient estimation error

Parameter	Value
$\mathbf{P}_0$	$\mathbf{I}_4$
$\mathbf{Q}_k$	$diag(0.98339\mathbf{I}_3, 0.00015631)$
$\mathbf{R}_k$	0.99992

Table 3: EKF parameters

of sound multiplicative coefficient estimation error. The initial state estimate was set to $\hat{\mathbf{x}}_0 = \begin{bmatrix}0 & 6 & 8 & 1.0\end{bmatrix}^T$. This represents an initial error of 10 meters in terms of position estimate and 0.1 in terms of the unknown coefficient estimate. As can be inferred, these initial conditions lead to a result fairly similar to that of the LKF, since both initial convergence and steady-state performance are comparable. Oppositely, a divergence of the position estimates error can be found in Fig. 6 (error of the speed of sound coefficient estimates are omitted due to space limitations). This was a result of changing the norm of the initial position error to 30 meters, while maintaining the speed of sound multiplicative coefficient error at 0.1. The initial assumption that lead to the diverging result was $\hat{\mathbf{x}}_0 = \begin{bmatrix}20 & 20 & 10 & 1.0\end{bmatrix}^T$.

As demonstrated, the EKF is a valid solution to solve the state estimation required for the navigation problem, since it yields converging results, although these can only be obtained when setting the initial state estimate close to the true initial state. Therefore, the EKF fails to provide global convergence guarantees.

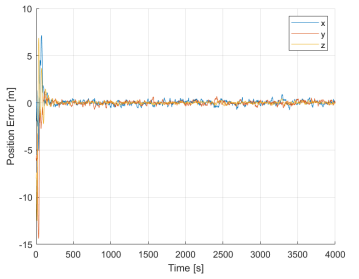

Figure 4: EKF position estimation error convergence

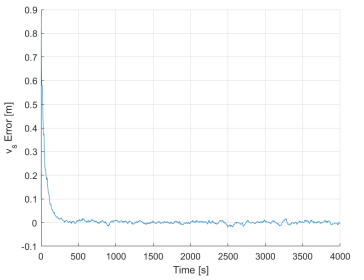

Figure 5: EKF speed of sound coefficient estimation error convergence

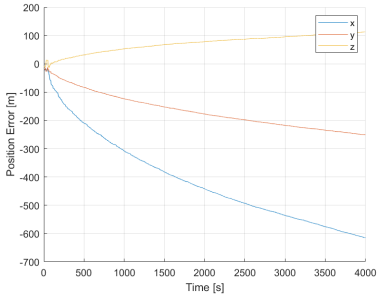

Figure 6: EKF position estimation error divergence

4.3. Unscented Kalman filter

Similarly to what was done for the LKF and the EKF, the process and measurement noise covariance matrices were determined resorting to the BO algorithm. The parameters used to feed the UKF are presented in Table 4.

Parameter	Value
$\mathbf{P}_0$	$\mathbf{I}_4$
$\mathbf{Q}_k$	$diag(0.032846\mathbf{I}_3, 0.0052031)$
$\mathbf{R}_k$	0.98731

Table 4: UKF parameters

As for the EKF, two sets of figures represent two distinct results obtained when using the UKF. Firstly, the initial condition which ultimately lead

to diverging state estimate errors when using the EKF, $\hat{\mathbf{x}}_0 = \begin{bmatrix}20 & 20 & 10 & 1.0\end{bmatrix}^T$, now results in a valid estimation process as depicted in Figures 7 and 8. This confirms that the UKF exhibits better performance than the EKF. Notice, however, that the transients take longer, increasing by a factor of ten when compared to the transients of the EKF. Secondly, Fig. 9 shows the errors of the position estimates obtained after simulating the filter with the initial condition $\hat{\mathbf{x}}_0 = \begin{bmatrix}100 & 141.42 & 141.42 & 1.0\end{bmatrix}^T$(errors of the speed of sound coefficient estimates are omitted due to space limitations). This time, although the UKF manages to attain error convergence, this happens at a very slow rate. In fact, convergence was only achieved after extending the simulation length to 100000 seconds (approximately 27 hours). Although this result does not depict a diverging estimation process, it shows that the UKF is rendered useless for some initial filter conditions.

To sum up, the UKF, like the EKF, is able to obtain valid estimation results, but lacks the capability to offer, in an acceptable time span, convergence guarantees for all initial conditions.

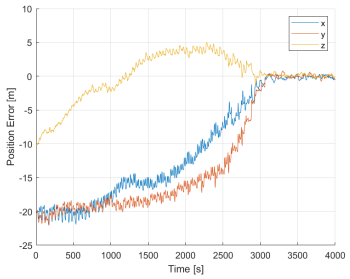

Figure 7: UKF position estimation error convergence

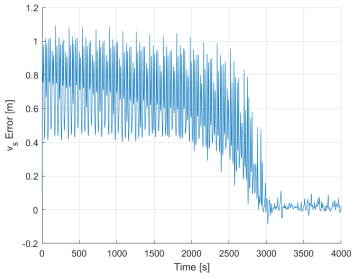

Figure 8: UKF speed of sound coefficient estimation error convergence

For comparison purposes, Table 5 presents the averaged steady-state ($t > 3000$s) estimation errors of each filtering solution.

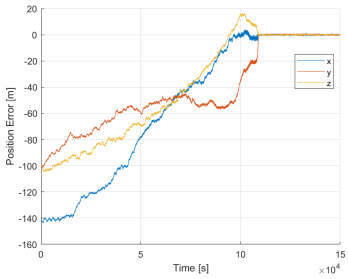

Figure 9: UKF position estimation error slow convergence

Filter	$\mathbf{p}^x[m]$	$\mathbf{p}^y[m]$	$\mathbf{p}^z[m]$	v_s
LKF	-0.0154	-0.0181	0.0313	0.0038
EKF	-0.0173	-0.0589	-0.0186	-0.0010
UKF	-0.0076	-0.0487	-0.0351	0.0122

Table 5: Steady-state estimation average error

4.4. Monte Carlo Simulations

To better assess the performance of each solution, Monte Carlo simulations were carried out. Each simulation comprised its own randomly generated noise signal and initial state, the later being portrayed by a Gaussian distribution centered about the true initial state and with covariance equal to the initial error covariance of the filter, $\mathbf{P}_0$. The covariance matrices used for each Kalman filter are expressed in Table 6. Note, in particular, that the

	LKF	EKF	UKF
Error Covariance	$\mathbf{I}_5$	$\mathbf{I}_4$	$\mathbf{I}_4$

Table 6: Initial state error covariance in the Monte Carlo simulations

variation allowed for the initial unknown coefficient, $\sigma^2_{v_S} = 1$, is a very liberal one. This makes for a very broad-scenario of initial v_s conditions when performing Monte Carlo simulations. A total of 1000 runs of each filtering process were performed.

The averaged steady-state ($t > 500s$) mean estimation error is portrayed in Table 7. All three filters show some bias, especially in the third position component, $\mathbf{p}^z$, and in the speed of sound multiplicative coefficient, v_s.

Filter	$\mathbf{p}^x[m]$	$\mathbf{p}^y[m]$	$\mathbf{p}^z[m]$	v_s
LKF	-0.0072	-0.0035	0.0133	0.0019
EKF	-0.0020	0.0029	0.0024	0.00045
UKF	-0.0266	-0.0072	0.0131	0.0151

Table 7: Monte Carlo steady-state estimation average error

The standard deviation of the estimation errors was determined and compared to the Bayesian Cramér-Rao bound. Table 8 shows the steady-state averaged standard deviations of the estimation error. All filters perform fairly close to the lower bound provided by the BCRB. Going into further detail, it can be seen that the EKF tends to consistently over-perform the BCRB. Also, for the speed of sound multiplicative coefficient, v_s, the LKF shows, on average, error standard deviations below the BCRB. These odd observations are explained by the biased nature of the filters. Since the BCRB only sets a lower limit on the error standard deviations for unbiased estimators, a biased estimator is allowed to achieve such results.

Filter	$\mathbf{p}^x[m]$	$\mathbf{p}^y[m]$	$\mathbf{p}^z[m]$	v_s
LKF	0.2864	0.2595	0.1796	0.0088
EKF	0.1992	0.1842	0.1091	0.0065
UKF	0.2908	0.2503	0.2083	0.0189
BCRB	0.2392	0.2165	0.1757	0.0173

Table 8: Monte Carlo steady-state averaged standard deviation of the estimation error

5. Experiments

Experiments were performed to further test the filtering solutions presented throughout this work. These were carried out at the Institute for Systems and Robotics installations, and consisted of a drone autonomously describing a trajectory inside a flight arena. Throughout the length of the experiment, flight measurements were acquired for *a posteriori* analysis.

The test arena is equipped with a motion capture system (MOCAP) and off-board computers capable of controlling drone position to a continuous trajectory function [15]. As the trajectory presented in Section 4 exceeded arena bounds, it was modified to

$$\mathbf{p}'(t) = \begin{bmatrix} 1.6cos\left(\frac{2\pi}{30}t\right) \\ 2.6cos\left(\frac{\pi}{10}t + \frac{\pi}{6}\right) \\ 1.2 + 0.6cos\left(\frac{2\pi}{45}t + \frac{\pi}{9}\right), \end{bmatrix}, \qquad (19)$$

where $t > 0 \in \mathbb{R}$ is the continuous variable representative of the time elapsed since the start of the trajectory. The full experiment lasted for approximately five minutes. This included the movement between the initial position, set by hand close to the center of the reference frame, and $\mathbf{p}'(0)$, and that between the final point of $\mathbf{p}'(t)$ and the stopping point on the ground. A plot of the trajectory is shown in Fig. 10.

Two completely independent systems were used to acquire both measurements needed to implement

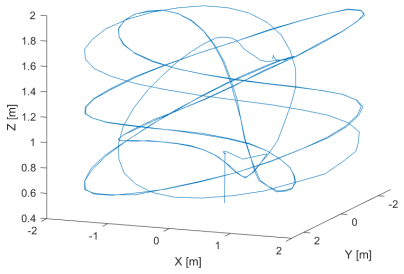

Figure 10: Experimental trajectory

either of the three filters discussed in the previous sections. The pseudo-ranges, $r(k)$, were acquired by an off-the-shelf acoustic "Indoor Positioning and Navigation System" offered by Marvelmind Robotics™ [16]. Regarding the position variations, $\mathbf{u}(k)$, these were obtained through the motion capture system present in the arena. Although discrete-time inertial position variations could have been obtained directly from the MOCAP system, a more realistic approach was implemented. This consisted on both Euler angles and vehicle inertial velocity, expressed in body coordinates, being acquired in order to compute said position variations. A more in-depth look into measurement acquisition and computation follows.

5.1. Measurements

As said before, pseudo-range measurements were acquired by implementing a simple solution based on an off-the-shelf product. The non embarked beacon was placed on the floor of the arena in the inertial coordinates $\mathbf{s} \approx \begin{bmatrix} -2.31 & -0.10 & 0.01 \end{bmatrix}^T [m]$. Regarding the update rate of these measurements, this was set to 1 Hz.

To determine the position variations, $\mathbf{u}(k)$, the MOCAP system was used. This provides numerous flight parameters sampled at a frequency of 30 Hz. The set of used flight parameters comprises vehicle inertial velocity, expressed in body-coordinates, and orientation, given in terms of roll (ϕ), pitch (ψ), and yaw (θ), more commonly known as Euler angles. The position variations, were computed at a frequency of 1 Hz (to match the pseudo-range measurements frequency). As both the rotation matrices (computed with the Euler angles) and the velocities needed to determine the integral are available in discrete-time instants, the integral (5) can only be approximated through a sum. To that end, the trapezoidal rule was employed.

Euler angles and vehicle velocities were assumed to be corrupted by zero-mean white Gaussian noise with the standard deviations present in Table 9.

Measure	Standard deviation
Pseudo-ranges	10^{-2}m
Roll (ϕ)	0.03°
Pitch (ψ)	0.03°
Yaw (θ)	0.3°
Velocity	0.01m/s

Table 9: Standard deviation of the noise

5.2. Results

All three filters were tested, each with different settings. Each filter was initialized with a position error on coordinate x. The input noise covariance matrices were subject to the Bayesian optimization process. Table 10 summarizes all input parameters. Notice that, besides covariance matrix inputs being different for each filter, also the initial state estimate differs from the LKF to both the EKF and UKF, since too large initial state errors lead to non-converging results in the latter two, as seen in Subsections 4.2 and 4.3.

The MOCAP system also provides the actual position of the drone along the trajectory, which can be considered as the ground truth. This allows for the determination of the position estimation errors shown in Figures 11, 12 and 13. The better performing solution is clearly the LKF since, even having started with an initial error an order of magnitude above that of competing solutions, it leads

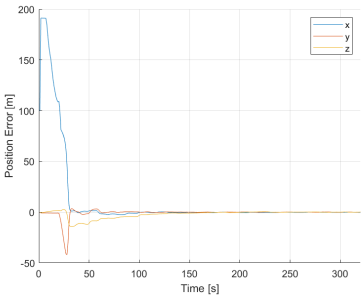

Figure 11: LKF position estimation error

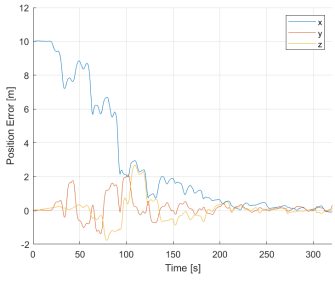

Figure 12: EKF position estimation error

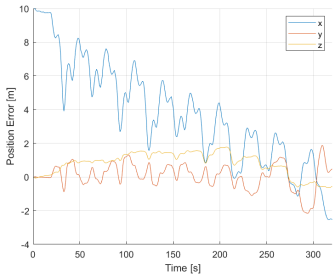

Figure 13: UKF position estimation error

to fast estimation error convergence while attaining remarkable steady-state performance, with errors contained within a margin of centimeters. It can also be seen that the EKF performs worse than the LKF. However, it could be used as a viable way to perform estimation in situations where there is a good knowledge of the true initial position. Finally, the UKF represents the worst performing solution since, within the time span of the experience (approx. 5 min), it could not manage to lead state estimates to their true values. Notice, however, this result is in accordance with what was concluded on Subsection 4.3 about the convergence rates of the UKF.

The estimates of the speed of sound unknown multiplicative coefficient using the LKF are shown in Fig. 14. No error can be computed to evaluate this particular estimate as true speed of sound in the arena is not available; only rough estimates based on temperature could have been performed. Nevertheless, it is clear that the coefficient estimates tend to a value of approximately 1.05, thus confirming the expected operation of the filter. To further confirm the proper functioning of the speed of sound multiplicative coefficient estimation, an artificial multiplicative error of 1.1 was applied to the pseudo-range measurements acquired by the Marvelmind™system. The results presented in Fig. 15 show an approximate 10% increase in the steady-state speed of sound multiplicative coefficient estimates in comparison to those obtained without

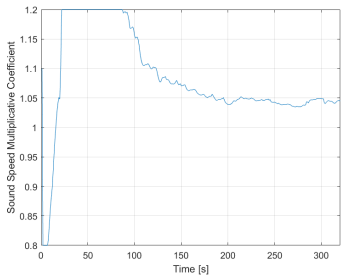

Figure 14: LKF speed of sound multiplicative coefficient estimation results

	LKF	EKF	UKF
Q_k	$diag(0.2405\mathbf{I}_3, 0.0021, 0.0125)$	$diag(0.7264\mathbf{I}_3, 00120)$	$diag(0.8172\mathbf{I}_3, 0.0020$
R_k	0.6922	0.9982	0.2535
$\mathbf{P}_0$	$\mathbf{I}_5$	$\mathbf{I}_4$	$\mathbf{I}_4$
$\hat{\mathbf{p}}_0 - \mathbf{p}_0$	$\begin{bmatrix}100 & 0 & 0\end{bmatrix}^T [m]$	$\begin{bmatrix}10 & 0 & 0\end{bmatrix}^T [m]$	$\begin{bmatrix}10 & 0 & 0\end{bmatrix}^T [m]$

Table 10: Experimental filter input parameters

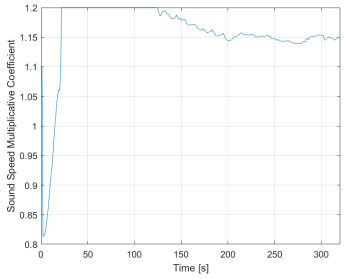

Figure 15: LKF speed of sound multiplicative coefficient estimation results with artificial pseudo-range input

artificial pseudo-range inputs. Hence, the proper functioning of the LKF is confirmed.

6. Conclusions

The novel solution proposed in this thesis provides position and unknown speed of sound multiplicative coefficient estimates with errors that tend rapidly to zero, while achieving respectable steady-state performance. Its major advantage is the fact that it has mathematically proven globally exponentially stable error dynamics. This is something that neither the EKF nor the UKF, used to compare this approach to, is able to provide. Monte Carlo simulations showed that the average steady-state estimation errors are well condensed within a thin margin. Nevertheless, a small bias in all the filters was found. Regarding optimal performance, all the solutions showed error standard deviations close to the lower bound given by the Baeysian Cramér-Rao bound. The experiments carried out in the test arena showed that the new solution can be seen as a viable method to perform vehicle navigation, even when the initial position of the vehicle is poorly determined. Further work on this subject could be done by projecting and executing a new experiment with real underwater vehicles equipped with inertial measurement units. This configuration would unequivocally demonstrate the true potential of the new solution when applied to real-life situations.

References

[1] Mikael Bliksted Larsen. Synthetic long baseline navigation of underwater vehicles. *Oceans Conference Record (IEEE)*, 3:2043–2050, 2000.

[2] A S Gadre and Daniel Stilwell. *Toward underwater navigation based on range measurements from a single location*, volume 5. jan 2004.

[3] Aditya S. Gadre and Daniel J. Stilwell. Underwater Navigation In the Presence of Unknown Currents Based On Range Measurements From a Single Location. In *American Control Conference*, volume 2, pages L.02–L02, 2005.

[4] A S Gadre and Daniel Stilwell. *A complete solution to underwater navigation in the presence of unknown currents based on range measurements from a single location*. sep 2005.

[5] Jérôme Jouffroy and Johann Reger. An algebraic perspective to single-transponder underwater navigation. *Proceedings of the IEEE International Conference on Control Applications*, pages 1789–1794, 2006.

[6] Pedro Batista, Carlos Silvestre, and Paulo Oliveira. Single range aided navigation and source localization: Observability and filter design. *Systems and Control Letters*, 60(8):665–673, 2011.

[7] Giovanni Indiveri, Daniela De Palma, and Gianfranco Parlangeli. Single Range Localization in 3-D: Observability and Robustness Issues. *IEEE Transactions on Control Systems Technology*, 24(5):1853–1860, 2016.

[8] Giovanni Indiveri. An Entropy-Like Estimator for Robust Parameter Identification. *Entropy*, 11, 2009.

[9] Pedro Batista. Navigation and source localization based on single pseudo-ranges. *Proceedings of the American Control Conference*, 2020-July:5237–5242, 2020.

[10] Hong-De Qin, Xiang Yu, Zhong-Ben Zhu, and Zhong-Chao Deng. An expectation-maximization based single-beacon underwater navigation method with unknown ESV. *Neurocomputing*, 378:295–303, 2020.

[11] Hong-De Qin, Xiang Yu, Zhong-Ben Zhu, and Zhong-Chao Deng. A variational Bayesian approximation based adaptive single beacon navigation method with unknown ESV. *Ocean Engineering*, 209:107484, 2020.

[12] Pedro Batista. GES long baseline navigation with unknown sound velocity and discrete-time range measurements. *IEEE Transactions on Control Systems Technology*, 23(1):219–230, 2015.

[13] Andrew H. Jazwinski. *Stochastic Processes and Filtering Theory*. 1970.

[14] Ibai Roman, Josu Ceberio, Alexander Mendiburu, and Jose A. Lozano. Bayesian optimization for parameter tuning in evolutionary algorithms. *2016 IEEE Congress on Evolutionary Computation, CEC 2016*, pages 4839–4845, 2016.

[15] Tiago Oliveira. Rapid Development and Prototyping Environment for Testing of Unmanned Aerial Vehicles, 2020.

[16] Marvelmind Robotics. Precise (±2cm) Indoor Positioning and Navigation for autonomous robots, drones, vehicles and humans.